Document downloaded from:

http://hdl.handle.net/10251/160613

This paper must be cited as:

García-Fayos, J.; Sogaard, M.; Kaiser, A.; Serra Alfaro, JM. (2019). Oxygen permeation studies in surface Pd-activated asymmetric Ce0.9Gd0.1O1.95 membranes for application in CO2 and CH4 environments. Separation and Purification Technology. 216:58-64. https://doi.org/10.1016/j.seppur.2019.01.068

The final publication is available at

https://doi.org/10.1016/j.seppur.2019.01.068

Copyright Elsevier

Additional Information

Oxygen permeation studies in surface Pd-activated asymmetric $Ce_{0.9}Gd_{0.1}O_{1.95}$ membranes for application in CO_2 and CH_4 environments

Julio Garcia-Fayos[1], Martin Søgaard[2], Andreas Kaiser[2], Jose M. Serra*[1]

[1] *Instituto de Tecnología Química (Universitat Politècnica de València – Consejo Superior de Investigaciones Científicas), av. Los Naranjos s/n, E-46022 Valencia, Spain*

[2] *Department of Energy Conversion and Storage, Technical University of Denmark, Risø campus, Frederiksborgvej 399, DK-4000 Roskilde, Denmark*

** Corresponding author. Tel: + 34.963879448 E-mail: jmserra@itq.upv.es*

Abstract

Oxygen Transport Membranes (OTMs) present a high potential for being considered in the integration of O_2 supply systems in oxyfuel installations, as well as for the conduction of chemical reactions when operating Catalytic Membrane Reactors (CMRs). Several solutions are being prospected for overcoming the main drawbacks regarding materials stability and membrane performance. A highly stable material such as $Ce_{0.9}Gd_{0.1}O_{1.95}$ (CGO) doped with 2% mol. Co was studied as a 40 μm thick CGO supported CGO membrane. This membrane was characterized by studying its performance as oxygen permeation membrane for the production of oxygen under oxyfuel conditions and for the conduction of chemical reactions involving CH_4. In order to improve oxygen surface reactions and consequently, the oxygen permeation, the membrane was surface activated with the addition of Pd nanoparticles. A broad characterization consisting of the study of O_2 production under different environments simulating real application conditions was conducted by subjecting the membrane to Ar, CO_2 and CH_4 environments in the temperature range of 750 to 1000 ºC. A peak oxygen flux of 7.8 $ml \cdot min^{-1} \cdot cm^{-2}$ was obtained at 1000 ºC when using a sweep consisting of 75% CH_4 in Ar. This flux corresponds to a 16-fold improvement in the O_2 permeation at 1000 ºC when sweeping with Ar, with an oxygen flux of 0.47 $ml \cdot min^{-1} \cdot cm^{-2}$. An oxygen flux of 1.2 $ml \cdot min^{-1} \cdot cm^{-2}$ was obtained at 1000 ºC when feeding with pO_2 = 1 atm in feed side. Membrane performance under CO_2-containing environments showed a positive effect of CO_2 on permeation at 1000-900 ºC, reaching up to 0.59 $ml \cdot min^{-1} \cdot cm^{-2}$ O_2 at 1000 ºC. A continuous exposure of CO_2 during 48 hours at 750 ºC resulted in a slight $J(O_2)$ increase, with a reversible reduction in performance when returning to clean conditions, thus demonstrating high stability of CGO membranes.

Keywords: cerium gadolinium oxide, supported membrane, catalyst; tape casting, MIEC; syngas; oxyfuel

1. Introduction.

Nowadays, 68.1% of the electric power is generated from fossil fuel combustion, with 41.6% coal as the main exploited source [1]. This high percentage of fossil fuel combustion generated a CO_2 emission of 31,102.3 Mtons in 2010 [2] for satisfying the world electricity demand. Furthermore, some estimations predict that this

amount will increase to 40,226 Mtons in 2040 [1]. Since CO_2 is well-known for its direct contribution to greenhouse effect, increasingly more restrictive policies have been applied within the last two decades for limiting CO_2 gas emissions and, especially, for promoting processes and technologies which avoid CO_2 to be released to the atmosphere. Amongst the existing technologies, those that better fit the aforementioned requirements are based on strategies for the capture and sequestration of CO_2 from exhaust gases. Nevertheless, for being able to capture of CO_2, the exhaust gas has to be composed of a high percentage by CO_2. Enrichment of CO_2 in the exhaust gas is not possible if air is used in the combustion because of the high amounts of N_2 as well as presence of CO and NO_x hinder a proper CO_2 separation [3]. This situation can be solved by using pure O_2 following the oxyfuel combustion approach [4], where a flue gas stream mainly composed by CO_2 and H_2O is obtained, thus facilitating the separation and capture of CO_2.

The main drawback that is averting oxyfuel technology from being applied in most combustion processes is related to the supply of O_2. Currently, O_2 is produced by cryogenic distillation of air, which is a high-energy demanding process that requires the operation at very low temperatures and very high pressures in large plants. Therefore, cryogenic distillation is not economically viable for the most of existing power plants neither with the integration of air separation units, nor with the bulk O_2 provision from commercial suppliers in the high volumes for fuel combustion. An appealing solution for this supply of O_2 in small and medium scale applications can be found within Oxygen Transport Membranes (OTM), which are gas separation membranes consisting of metallic oxides presenting Mixed Ionic-Electronic Conductivity (MIEC) at high temperatures (>600 ºC). The main feature of MIEC materials is the ability of diffusing O^{2-} ions throughout their crystal lattice from a high to a low pO_2 side with a theoretical infinite selectivity. Due to the thermal requirement for conducting the O_2 separation, integrated OTM modules can benefit from waste heat streams generated in high temperature processes (e.g. oxyfuel and gasification plants), thus increasing plant efficiency. Therefore, if OTM modules are conveniently integrated in an oxyfuel power plant, an O_2-rich stream can be produced in-situ for achieving a complete fuel combustion to CO_2 and H_2O. MIEC materials presenting higher O_2 permeation rates are perovskites with formula $ABO_{3-\delta}$, comprising alkali-earth metal cations in the A-position. Nevertheless, these materials suffer from chemical and mechanical instability due to carbonation under CO_2-containing environments, making them unsuitable for oxyfuel applications [5, 6].

A solution for the application of MIEC materials in oxyfuel environments can be found amongst lanthanide doped ceria materials, since they present a combination of high oxygen-ion mobility and chemical compatibility with H_2O and CO_2 at high temperatures. Interesting results have been obtained with gadolinium doped ceria ($Ce_{0.9}Gd_{0.1}O_{1.95}$, CGO) in terms of O_2 permeability when tested under conditions representative of syngas and oxyfuel applications [7, 8] and for oxygen separation [9]. However, such observed O_2 fluxes are not enough for satisfying the requirements of practical applications. This lack in performance, which is due to the low electronic conductivity of CGO, can be improved by following several strategies: (1) by combining CGO with pure electronic conducting materials in dual-phase structures [10-16], (2) by reducing membrane thickness [7, 8], and (3) by improving oxygen surface reactions with active catalysts [8]. Additionally to the high O^{2-} mobility, lanthanide doped ceria materials also present red-ox catalytic properties, which are very suitable for the conduction of alkane oxidation reactions [17-20]. The exploitation of these features expands the potential industrial applications of ceria-based membranes if integrated as Catalytic Membrane Reactors (CMRs). The main interest of this approach is the production of syngas and valuable base chemicals such as ethylene and propylene.

The present work studies the potential use of asymmetric CGO membranes with 2% mol. of Co and surfaces activated with Pd nanoparticles for oxyfuel and chemical production production applications. A thorough study was conducted for determining the influence of temperature, pO_2 gradient, support porosity, CO_2 and CH_4 content on O_2 permeation.

2. Experimental.

Asymmetric CGO membranes were prepared at Risø National Laboratory for Sustainable Energy by tape casting, lamination and subsequent co-sintering and cutting. The slurries for the tape casting of the porous support and the membrane were prepared by ball milling in ethanol a CGO powder (Rhodia S.A.,France), a PVB based binder system and a polyethylene imine (PEI, branched, M.W. 10,000, 99% Alfa Aesar) as a dispersant. 2 mol.% of Co nitrate (cobalt(II) nitrate hexahydrate, 97.7% min, Alfa Aesar) was added as a sintering aid after drying. Graphite was used for porosity promotion of CGO support in a 5% vol. (V-UF1, 99.9, Graphit Kropfmühl AG, Germany) being added to the slurry for tape casting. Once the layers of both the thin film CGO membrane and the porous CGO support were tape casted, these were combined by lamination by applying heat and pressure on to the tapes between two rolls. Membrane rounds of about 34 mm diameter were stamped out from the green membrane multilayer tapes before sintering. In a binder

removal step the organics were removed by a very slow de-bindering profile to avoid damage of the structure. Subsequently, the structure was sintered in air at 1300 °C for 2 hours. After sintering, the membrane structures were laser-cut to the exact final dimensions (diameter of 15 mm).

Surface activation of CGO membrane was conducted by addition of Pd nanoparticles by dropping a 1 M solution containing a Pd precursor (Pd nitrate dyhidrate) onto the membrane surface. After deposition, the catalytic coating was dried at 80 ºC during 1 hour and final sintering was performed in-situ once the membrane was located in the experimental set for the conduction of the oxygen permeation tests.

Identification of the crystalline phases of the samples was done by means of X-ray diffraction (XRD). The measurements were carried out using a PANalytical CubiX fast diffractometer, using CuKα1 radiation (λ = 1.5406 Å) and a X'Celerator detector in Bragg−Brentano geometry. XRD patterns recorded in the 2θ range from 10° to 90° were analyzed using X'Pert Highscore Plus software. Field Emission Scanning Electron Microscopy (FESEM) and Energy-dispersive X-ray spectroscopy (EDX) analyses were performed using a ZEISS Ultra55 field emission scanning electron microscope.

Raman spectra were measured with a Renishaw inVia Raman spectrometer equipped with a Leica DMLM microscope and a 514-nm Ar+ ion laser as an excitation source. A x50 objective of 8-mm optical length was used to focus the depolarized laser beam on a spot of about 3 μm in diameter. The Raman scattering was collected with a charged coupled device (CCD) array detector.

Oxygen permeation studies were carried in a laboratory scale quartz reactor. Synthetic air (21% O_2 in N_2), mixtures of O_2 and He (21%, 50% and 75% O_2 in He) or pure O_2 were fed into the oxygen-rich chamber, while argon, and dilutions of CO_2 and CH_4 in argon were used as the sweep gas on the permeate side. Feed gas streams were fed in the porous support side, whereas sweep gases were fed on the dense membrane layer side. The gas flows were 300 ml·min^{-1} for feed and sweep streams, which were fed at atmospheric pressure. All streams were individually mass flow controlled. The temperature was measured by a thermocouple attached to the membrane. A PID controller maintained temperature variations within 2 ºC of the set point. The samples consisted of 15 mm diameter disk-shaped gastight membranes and membrane gas leak-free conditions were achieved using gold rings, which were heated to > 1000 ºC. The permeate was analyzed at steady state by online gas chromatography using a micro-GC Varian CP-4900 equipped with Molsieve5A, Pora-Plot-Q glass capillary, and CP-Sil modules. Membrane gas leak-free conditions were ensured by continuously monitoring the N_2 concentration in the product gas stream. The data reported were achieved at steady state after 1 h in the reaction stream. Each GC analysis was repeated three times to minimize the analysis error. The experimental analytical error was below 0.5%.

3. Results and discussion.

3.1. Microstructure of the membrane assembly.

Prior to testing, a microstructural characterization on a fresh asymmetric CGO membrane was performed by means of FESEM, EDX and XRD. The membrane assembly can be identified in Figure 1a, where a cross-section view shows a uniform and homogenous 40 μm-thick dense CGO layer deposited on a CGO porous support. Surface view depicted in Figure 1b evidences a distribution of packed CGO grains with sizes between 100 and 700 nm. No holes and pinholes are observed, thus ensuring a membrane gas tightness that was confirmed by a He-leak test. With regard to porous substrate, in Figure 1c it is observed a well-interconnected and homogenous pore distribution with pore sizes of 0.5-3 μm and a porosity degree of 20-25% (estimated from image analysis with ImageJ software). CGO membrane composition was confirmed by XRD measurements, with no appearance of any secondary phase or impurities (Figure S1). Despite being doped with 2% mol. of cobalt, no signs of Co species were observed in XRD measurements, this can be ascribed to the fact that Co loading is below device detection limit. Nevertheless, a good Co distribution in the CGO matrix can be expected as previously observed in [17]. Surface activation with Pd nanoparticles can be observed in Figure 1d with a dispersion of Pd particles (light grey grains) covering ca. 20% of membrane surface, and presenting particle sizes of <200 nm and with some particle agglomerates exceeding 1 μm. The composition of these nanoparticles was analysed by EDX (Figure S2) confirming they consisted of Pd.

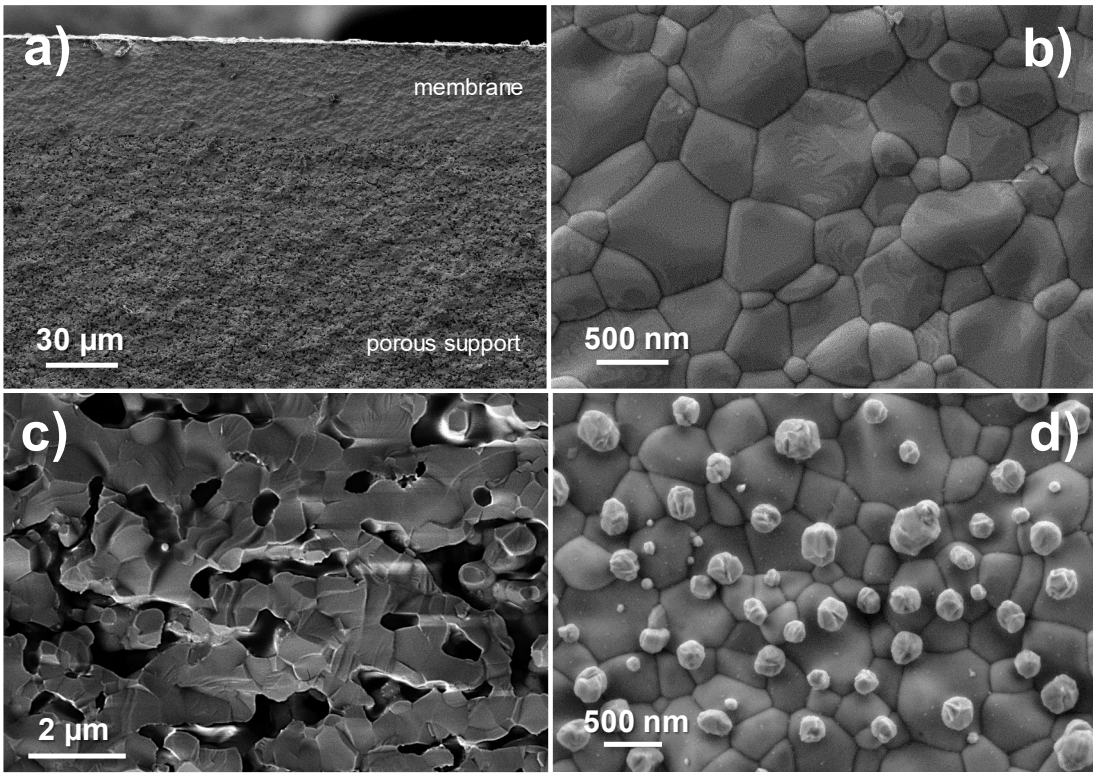

Figure 1: FESEM images of an as fabricated asymmetric CGO membrane: a) Membrane fracture cross section, b) surface of CGO dense top layer (without surface activation), c) Fracture cross section details of the porous support, and d) FESEM surface view of CGO dense top layer after activation with Pd.

3.2. Oxygen permeation tests.

The conduction of O_2 permeation tests was carried out on a CGO asymmetric membrane which was surface activated with Pd nanoparticles for boosting the oxygen oxidation reactions (OOR) that take place at the surface of the permeate side. A characterization of the membranes was conducted for studying the membrane performance under different application representative environments. Furthermore, some studies were performed for determining the influence of the porous support on the feed gas diffusion to membrane surface, and the effect of CO_2 and CH_4 content in the oxygen permeation.

Temperature and sweep gas dependence.

Different environments were considered for studying the oxygen permeation through the asymmetric CGO membranes: (i) clean conditions (argon sweeping), (ii) oxyfuel conditions (CO_2 sweeping) and (iii) syngas production conditions (10% CH_4 in argon sweeping). Beneath the investigation of the oxygen flux, $J(O_2)$, in these different environments, the effect of temperature was also studied within the temperature range of 750 to 1000 ºC. The results displayed in Figure 2 show an oxygen flux of 0.47 $ml \cdot min^{-1} \cdot cm^{-2}$ at 1000 ºC when sweeping with Ar, whereas at lower temperatures the $J(O_2)$ drops to 0.17 and 0.031 $ml \cdot min^{-1} \cdot cm^{-2}$ at 900 and 750 ºC, respectively. When testing under pure CO_2 sweeping conditions, the results show an increase in $J(O_2)$ to 0.59 $ml \cdot min^{-1} \cdot cm^{-2}$ at 1000 ºC. Regardless it could be expected a $J(O_2)$ drop due to competitive adsorption between CO_2 and O_2 on surface actives sites, this improving effect of CO_2 has been previously observed in previous studies [21-24] and can be ascribed to a better sweeping properties of CO_2 at high temperatures (>900 ºC). This can be related to the higher thermal emissivity of CO_2 with respect to Ar, which can produce a local increase in membrane surface temperature, and subsequently in the oxygen permeation. A maximum O_2 flux of 2.76 $ml \cdot min^{-1} \cdot cm^{-2}$ is obtained at 1000 ºC when sweeping with 10% CH_4 in argon. This significant improvement in O_2 permeation is due to the partial reduction of Ce^{+4} to Ce^{+3} which implies an increase n-type electronic conductivity and subsequently an increase in ambipolar conductivity [8]. Furthermore, the induction of reducing environments produces a reduction of pO_2 at permeate side in comparison with argon. This reduction in pO_2 results in a higher pO_2 gradient through membrane thus increasing driving force and eventually implying a gain in $J(O_2)$ [25].

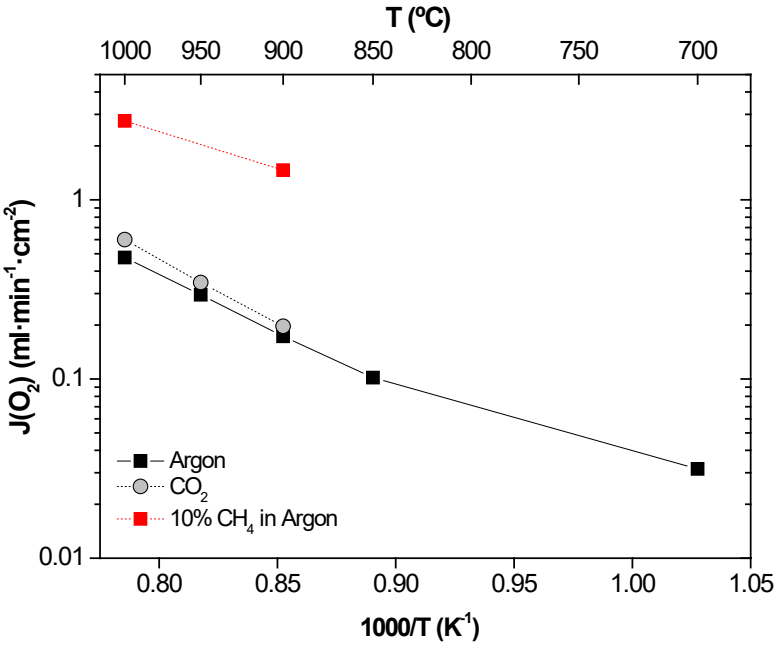

Figure 2: Dependence of oxygen permeation on temperature under different sweep environments: Ar, CO_2 and 10% CH_4 in Ar. Synthetic air used as feed in all the cases. The gas flows were 300 ml·min[1] for feed and sweep in all cases.

Effect of oxygen partial pressure in feed stream.

According to Wagner equation[1], the O_2 permeation through OTMs depends directly on the pO_2 gradient between the two sides of membrane, in the way that the larger the difference between pO_2 at the feed and sweep side is, the higher is the O_2 permeation. Therefore, the performance of CGO membranes was tested under different pO_2 gradients by varying the oxygen partial pressure in the feed stream from 0.21 to 1 atm while maintaining a constant argon sweep gas flow of 300 ml·min^{-1}. Moreover, for studying the influence of porous support on the feed gas diffusion different mixtures consisting of 21% O_2 in N_2 (synthetic air) and 21% O_2 in He where used as feed gas (pO_2 = 0.21 atm). Results displayed in Figure 3 show that feeding with a O_2/He mixture a higher $J(O_2)$ is achieved than when O_2 is diluted with N_2 (void symbols). A flux of 0.57 ml·min^{-1}·cm^{-2} O_2 is obtained when using He and 0.47 ml·min^{-1}·cm^{-2} O_2 when diluting with N_2 at 1000 ºC. This is ascribed to a faster diffusion of O_2 in He through the porous support due to the low molecular size of He, resulting in a lower gas diffusion limitation, and subsequently in more paths for O_2 to diffuse through the substrate [21]. These results are a sign of the limitation of the support porosity towards gas diffusion and eventually towards O_2 permeation; therefore a higher porosity degree would produce a beneficial effect in membrane performance.

A peak $J(O_2)$ of 1.2 ml·min^{-1}·cm^{-2} is obtained at 1000 ºC when feeding with pure O_2, representing a 2.5-fold increase in permeation with respect to air feeding. At 700ºC, oxygen fluxes corresponding to pO_2 between 0.5-1 atm, were in the range 0.16-0.21 ml·min^{-1}·cm^{-2}. Figure 3 depicts the $J(O_2)$ in dependence of pO_2 in feed for each given temperature in the range 1000-700ºC; two main conclusions can be formulated from the observation of the results: (i) higher pO_2 in feed side yield higher $J(O_2)$, and (ii) at higher temperatures, pO_2 increments result in higher permeation improvement. This is in agreement with Wagner equation, since $J(O_2)$ improve more with pO_2 in the high T region due to the bulk diffusion limitation. Subsequently, O_2 permeation tests carried out at 700ºC would be limited by surface exchange processes, given that increasing pO_2 at feed side hardly improves $J(O_2)$ even if using pure O_2.

[1] $J_{O2} = \frac{RT}{16F^2L}\int_{P''_{O2}}^{P'_{O2}} \sigma_{amb}(pO_2)dlnpO_2$, where J_{O2} is the oxygen permeation flux in mol·m^{-2}·s^{-1}, R is the gas constant, F is the Faraday constant, L is the membrane thickness, σ_{amb} is the ambipolar conductivity, and P'_{O2} and P''_{O2} are the oxygen partial pressures at the high pressure side and low pressure side, respectively.

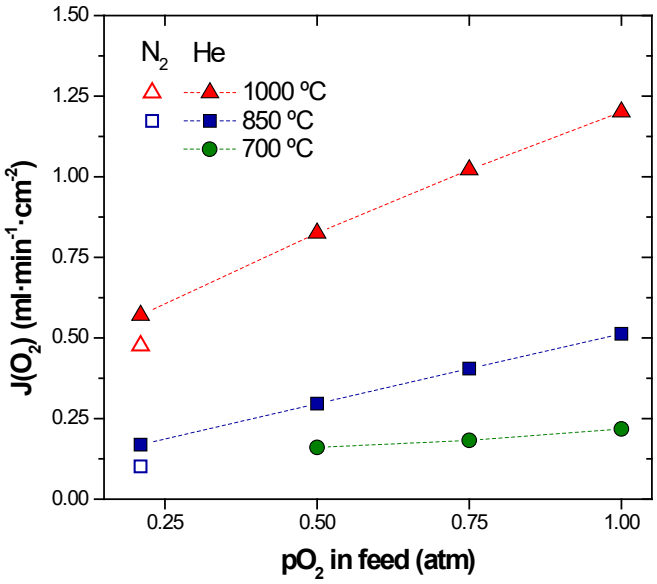

Figure 3: Oxygen permeation through an asymmetric, Pd-activated CGO membrane operated with different feed stream compositions at different temperatures. Argon sweeping in all the cases. Fill symbols correspond to O_2/He mixtures whereas void symbols correspond to O_2/N_2 mixture. The gas flows were 300 ml·min^1 for feed and sweep in all cases.

Studies under oxyfuel conditions

In one of the most preferred configurations when integrating OTM modules in oxyfuel installations, the process exhaust gases are used for membrane sweeping. In this configuration the waste heat from the exhaust gas stream can be utilized for heating up the modules to operation temperature. The exhaust gases in an oxyfuel installation are mainly composed by CO_2 (>70% vol.), H_2O and O_2 (1-3% vol.). Thus the membrane materials should be chemical and mechanical stable under these harsh conditions. The effects of CO_2 exposure on the oxygen flux the asymmetric CGO membrane has been studied by applying different CO_2 concentrations in the sweep stream. Figure 4a shows the J(O_2) at 1000, 950 and 900 ºC when varying CO_2 content in sweep from 0 to 100%. As can be seen, in the considered T range the CO_2 content in the sweep stream improves the oxygen flux J(O_2) with increasing values at higher temperatures. At 1000 ºC J(O_2) increases from 0.5 to 0.59 ml·min^{-1}·cm^{-2} when switching from 0 to 100% CO_2, resulting in an improvement of ca. 18%. This effect is less marked at lower temperatures (950 and 900ºC). Since there is not expected any significant interaction between CO_2 and membrane surface (carbonation and competitive adsorption processes [26]) this improving effect can only be explained by different sweep gas properties, as previously reported [21, 22, 24, 27]. As previously mentioned, the higher thermal emissivity of CO_2 compared to Ar may increase oxygen permeation due to a local increase in temperature at membrane surface exposed to CO_2.

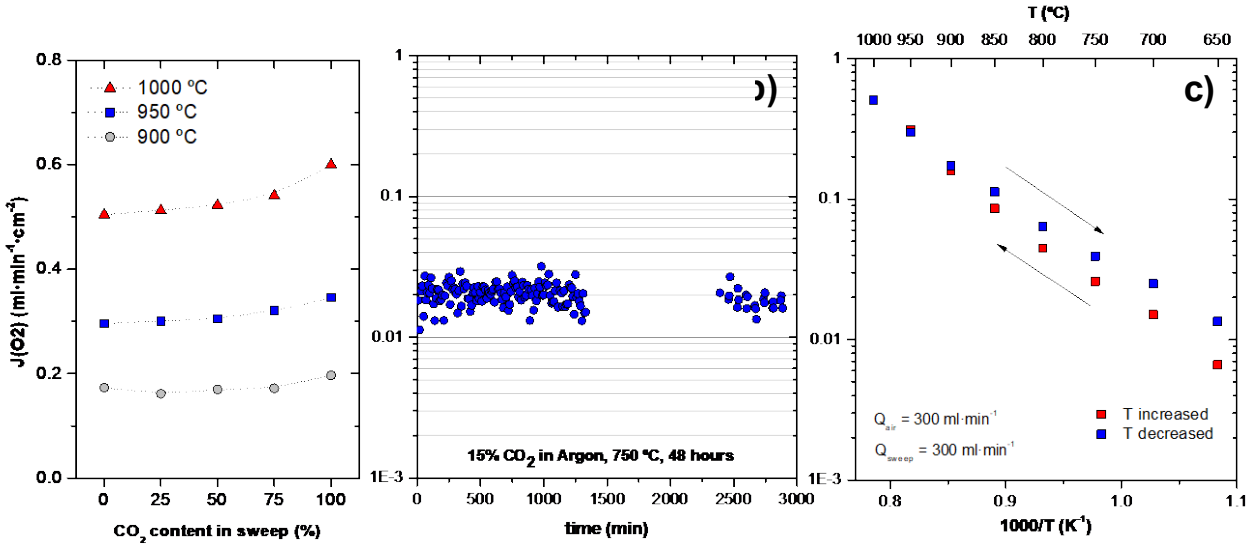

Figure 4: a) oxygen fluxes in dependence of CO_2 content in sweep stream at different temperatures- Air feeding (300 ml·min^{-1}), b) oxygen permeation evolution with time under Air/15% CO_2 in Ar gradient at 750 ºC, and c) effect of increasing temperature in J(O_2) after 48 hours exposition under 15% CO_2 in Argon.

In order to study the CO_2 poisoning resistance of CGO membrane, a CO_2-stability test was conducted at lower temperatures. The test procedure consisted of (i) expositing the membrane to a 15% CO_2 in argon sweep stream during a period of 48 hours at 750ºC, and then (ii) switching to pure clean conditions for checking membrane performance after CO_2 exposure. In this second step, the sweep is switched to Ar and the temperature is reduced to 650ºC, measuring afterwards the oxygen permeation J(O_2) in two consecutive steps: first rising temperature from 650 to 1000ºC, and then returning back from 1000 to 650ºC. A schematic diagram of this procedure is provided in Figure S3. Stability test results are shown in Figure 4b, where it can be seen that after 48 hours the oxygen flux, J(O_2), dropped from 0.022 to 0.018 ml·min^{-1}·cm^{-2} thus evidencing a slight loss of permeation under CO_2 atmosphere at 750ºC. This is confirmed by the results shown in Figure 4c, where O_2 fluxes are reduced when the temperature increases compared to the test when the temperature is decreased from high to low temperature. *J(O_2)* presents a value of 0.007 and 0.013 ml·min^{-1}·cm^{-2} before and after proceeding with test at 650 ºC, respectively. It can be concluded, that the CO_2 sweeping is affecting the CGO membrane performance immediately after exposure, whereas J(O_2) improves after increasing temperature to 1000ºC. The fact that above 900 ºC the O_2 fluxes are the same independent on the heating history, is indicative that species worsening O_2 permeation were formed during CO_2 stability test, being later decomposed or reacted into another when surpassing 900ºC. Another explanation could be related with a catalyst evolution after testing.

An analytical characterization was carried out on a Pd-impregnated CGO powder consisting of micron sized particles with the same composition as CGO membrane. Pd impregnation was conducted by incipient wetness impregnation using a palladium nitrate solution The impregnation load was set at 5% wt. Pd in order to achieve similar proportions as for the coating deposited on membrane surface. The Pd-impregnated powder was first sintered in air at 800 ºC for forming Pd nanoparticles phase. Then, the sintered powder was subjected during 48 hours to a 15% CO_2 in Ar stream at 750 ºC in a packed bed reactor, replicating the conditions of the CO_2-stability test. Then, it was performed XRD (Figure 5a) and Raman (Figure 5b) measurements of the powder sample before and after CO_2 treatment. XRD results are depicted in Figure 5a, where the powder sample before treatment presents a peak corresponding to Pd-O at 34.05º (★), which was disappearing after CO_2 treatment. Instead, peaks belonging to metallic Pd^0 (◆) were detected after CO_2 exposure. These results indicate that Pd di-nitrate used as Pd precursor is converted into PdO during sintering of the material at 800 ºC in air, and then is reduced into metallic Pd when exposed to CO_2. Measurements conducted by Raman spectroscopy on the same samples show similar results (Figure 5b) with an absorption band at 463.4 cm^{-1} that belongs to the Raman active F_{2g} mode vibration of CeO_2 [28, 29], an absorption band at 567 cm^{-1} attributed to O_2 vacancies and at 650 cm^{-1} [30] and a strong band corresponding to the Pd-O bond [31]. Results belonging to after treatment sample confirm Pd-O bond disappearance, which can be ascribed to the PdO reduction into Pd after CO_2 exposure observed in XRD results (Figure 5a). Therefore, one explanation for the lower permeation after CO_2 exposition can be related with the fact that Pd^0 nanoparticles present worse OOR catalytic properties than PdO, in addition to a probable change in the dispersion and morphology of the catalyst nanoparticles after exposition at high temperatures.

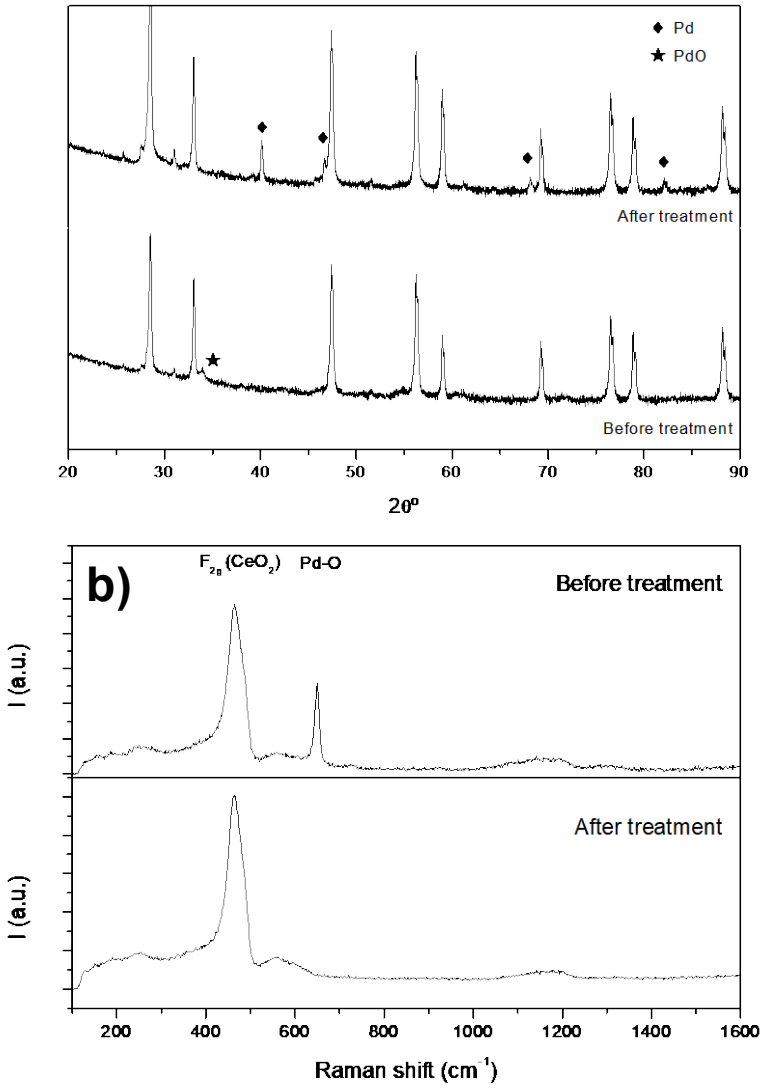

Figure 5: a) XRD measurements Pd-impregnated CGO powder before and after CO_2 annealing during 48 hours at 750 ºC, b) Raman spectra of Pd-impregnated CGO powder before and after CO_2 annealing.

Effect of CH_4 content in sweep stream.

The effect of CH_4 concentration on oxygen flux, $J(O_2)$, was also evaluated thus determining the performance of CGO membranes under highly reducing environments. These tests at 1000 ºC were conducted with varying CH_4 content in the sweep stream by considering different dilutions of CH_4 in Argon (10%, 25%, 50% and 75% of CH_4). As can be seen in Figure 6, a significant increase in $J(O_2)$ is achieved by only using 10% CH_4 obtaining 5 times the flux than when using pure Ar sweeping. Further increase in CH_4 concentration resulted in significantly higher O_2 fluxes with a peak of 7.8 $ml \cdot min^{-1} \cdot cm^{-2}$ at a concentration of 75% CH_4. This value represents a 16-fold improvement in the permeation at 1000 ºC compared to the oxygen flux obtained at the same temperature when sweeping with pure Ar. In conclusion, CGO membranes show very suitable performance for chemical reactions with CH_4, such as Partial Oxidation of Methane for the production of syngas, or Oxidative Coupling of Methane for obtaining ethylene.

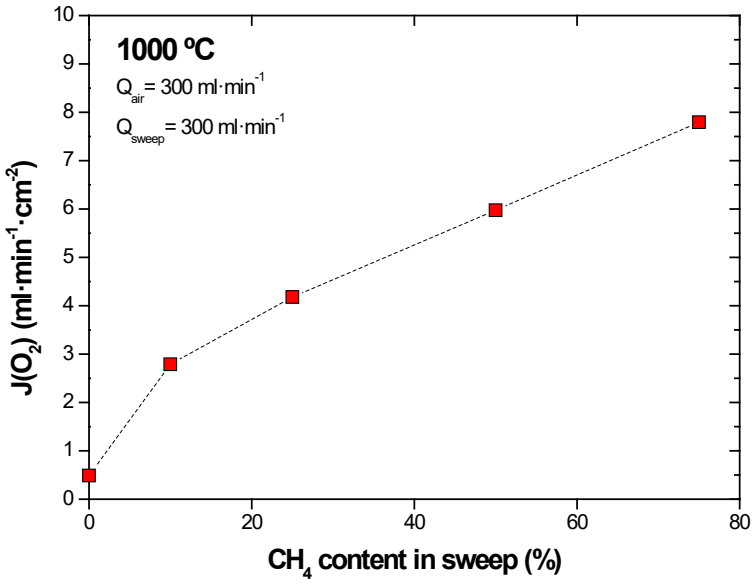

Figure 6: Influence of methane content (in sweep gas) on the oxygen permeation of a CGO membranes at 1000 ºC. Synthetic air was used as feed gas (300 ml·min^{-1}).

3.3. Post-mortem analysis.

Finally, a post-mortem characterization was performed on the tested membrane by XRD and FESEM. Figure 7 shows surface images of the as-prepared and tested membranes. As-prepared membrane was only exposed to an air atmosphere during catalyst sintering at 1050 ºC for 2 hours, whereas the tested membrane was subjected to different environments such as CO_2 and CH_4-containig atmospheres and temperatures in the range of 1060-650 ºC (see Figure S4). As can be seen in Figure 7, the initial Pd particles distribution on non-tested membrane (Figure 7a) changed after testing, presenting different morphology and distribution of the Pd particles (Figure 7b). Catalyst experienced a particle size growth of up to 200-500 nm and a reduction of coverage area to a 10% of membrane surface. Moreover, the CGO membrane surface presents a degradation consisting of the formation of holes of 0.5-1 μm diameter. Nevertheless, these holes do not represent a hazard to mechanical integrity of the dense layer since they are only affecting the membrane surface. The latter can be seen in cross-section shown in Figure 7c, where no degradation signs are visible in membrane layer. This surface degradation can be ascribed to a CGO reduction during CH_4 tests producing grain expansion phenomena and, eventually, to the release of some surface CGO grains. This release of grains may imply the loss of surface Pd particles attached to these grains as well. The presence of big Pd particles can be due to small Pd particles that coalesced with the time on stream during tests, as previously observed by Yacou et al. in the case of Pd-activated LSCF hollow fibres [32]. These two phenomena would explain the decrease in the surface coverage of Pd nanoparticles. Furthermore, XRD measurements performed on the tested membrane (Figure 7d) show no evidence of secondary phases generated from CGO reaction after testing, with only presence of Au peaks belonging to the sealing system employed for achieving leak-free conditions.

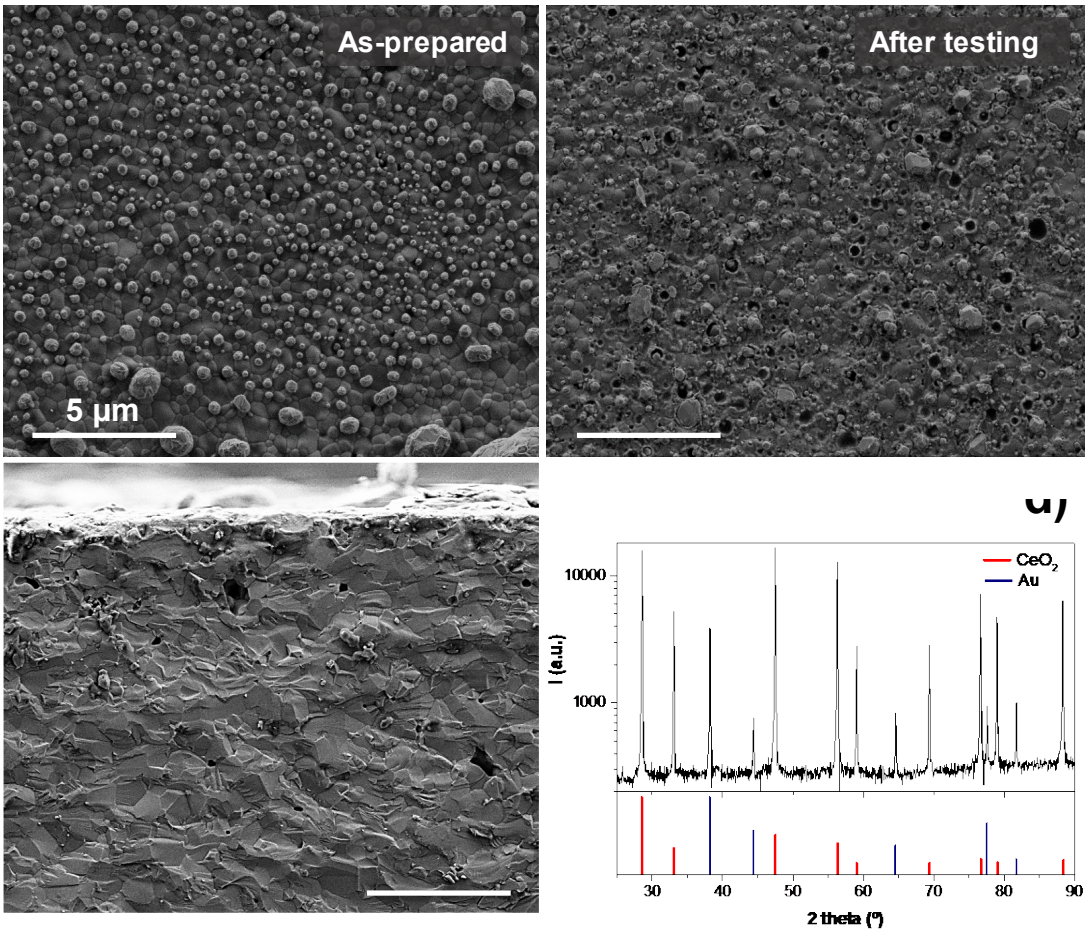

Figure 7: a) Surface SEM image of an as-prepared Pd-activated CGO membrane with the catalytic layer, b) surface of catalytic layer after membrane test and c) cross section pictures of a Pd-activated CGO membrane after test. d) XRD measurement of CGO membrane after test.

4. Conclusions.

A 40 µm thick CGO supported CGO membrane was characterized by studying its performance as oxygen permeation membrane for the production of oxygen under oxyfuel conditions and for the conduction of chemical reactions involving CH_4. In order to improve oxygen surface reactions and consequently, the oxygen permeation, the membrane was surface activated with the addition of Pd nanoparticles. A first microstructural evaluation of the asymmetric membrane confirmed a good membrane density with total absence of pores that can affect membrane gas tightness. This microstructural study also allowed the evaluation of the membrane assembly and the quantification of support porosity, resulting in a value of 20-25%. It was studied membrane behavior under different gradients representative of oxyfuel and syngas applications by testing membrane under Ar, CO_2 and CH_4 sweeping environments. When sweeping with Ar it is obtained a $J(O_2)$ of 0.47 $ml \cdot min^{-1} \cdot cm^{-2}$ at 1000 ºC, whereas 0.59 and 2.79 $ml \cdot min^{-1} \cdot cm^{-2}$ O_2 were obtained when sweeping with CO_2 and 10% CH_4 in Ar, respectively. pO_2 variation in feed side resulted in oxygen fluxes of 1.2 $ml \cdot min^{-1} \cdot cm^{-2}$ at 1000 ºC when feeding with pO_2 = 1 atm. The influence of CO_2 content on membrane performance was also studied, with a $J(O_2)$ upturn when sweeping with CO_2 at 1000 ºC and lower improvements as temperature was decreased to 900 ºC. The application of highly reducing environments resulted in an outstanding $J(O_2)$ of 7.8 $ml \cdot min^{-1} \cdot cm^{-2}$ when using a 75% CH_4 in Ar sweep gas, corresponding to a 16-fold improvement in the O_2 permeation at 1000 ºC when sweeping with Ar. Finally, a continuous exposure of CO_2 during 48 hours at 750 ºC resulted in a slight $J(O_2)$ decrease, with a reversible worsening in performance when returning to clean conditions. From the obtained results, CGO supported membranes can be considered as promising for applications presenting CO_2 and reducing environments. Though, the obtained $J(O_2)$ are still low for considering its use in practical applications. Further work on the catalytic activation, thickness reduction and assembly optimization would be required.

Acknowledgements

Financial support by the Spanish Ministry for Science and Innovation (Project ENE2008-06302) and by the EU through FP7 NASA-OTM Project (NMP3-SL-2009- 228701) is kindly acknowledged.

5. References.

[1] OECD, Electricity Generation, OECD Publishing.

[2] I.E. Agency, CO2 Emissions from Fuel Combustion 2012, OECD Publishing.

[3] C.R. Yoruk, A. Trikkel, R. Kuusik, Prediction of Flue Gas Composition and Comparative Overall Process Evaluation for Air and Oxyfuel Combustion of Estonian Oil Shale, Using Aspen Plus Process Simulation, Energy & Fuels, 30 (2016) 5893-5900.

[4] N. Perrin, R. Dubettier, F. Lockwood, J.-P. Tranier, C. Bourhy-Weber, P. Terrien, Oxycombustion for coal power plants: Advantages, solutions and projects, Applied Thermal Engineering, 74 (2015) 75-82.

[5] M. Arnold, H. Wang, A. Feldhoff, Influence of CO2 on the oxygen permeation performance and the microstructure of perovskite-type (Ba0.5Sr0.5)(Co0.8Fe0.2)O3−δ membranes, Journal of Membrane Science, 293 (2007) 44-52.

[6] A. Waindich, A. Möbius, M. Müller, Corrosion of Ba1−xSrxCo1−yFeyO3−δ and La0.3Ba0.7Co0.2Fe0.8O3−δ materials for oxygen separating membranes under Oxycoal conditions, Journal of Membrane Science, 337 (2009) 182-187.

[7] A. Kaiser, S. Foghmoes, C. Chatzichristodoulou, M. Søgaard, J.A. Glasscock, H.L. Frandsen, P.V. Hendriksen, Evaluation of thin film ceria membranes for syngas membrane reactors—Preparation, characterization and testing, Journal of Membrane Science, 378 (2011) 51-60.

[8] M.P. Lobera, J.M. Serra, S.P. Foghmoes, M. Søgaard, A. Kaiser, On the use of supported ceria membranes for oxyfuel process/syngas production, Journal of Membrane Science, 385–386 (2011) 154-161.

[9] H.J. Park, G.M. Choi, Oxygen permeability of gadolinium-doped ceria at high temperature, Journal of the European Ceramic Society, 24 (2004) 1313-1317.

[10] V.V. Kharton, A.V. Kovalevsky, A.P. Viskup, A.L. Shaula, F.M. Figueiredo, E.N. Naumovich, F.M.B. Marques, Oxygen transport in Ce0.8Gd0.2O2−δ-based composite membranes, Solid State Ionics, 160 (2003) 247-258.

[11] I. Kagomiya, T. Iijima, H. Takamura, Oxygen permeability of nanocrystalline Ce0.8Gd0.2O1.9–CoFe2O4 mixed-conductive films, Journal of Membrane Science, 286 (2006) 180-184.

[12] B. Wang, J. Yi, L. Winnubst, C. Chen, Stability and oxygen permeation behavior of Ce0.8Sm0.2O2−δ–La0.8Sr0.2CrO3−δ composite membrane under large oxygen partial pressure gradients, Journal of Membrane Science, 286 (2006) 22-25.

[13] J.S. Yoon, M.Y. Yoon, E.J. Lee, J.-W. Moon, H.J. Hwang, Influence of Ce0.9Gd0.1O2−δ particles on microstructure and oxygen permeability of Ba0.5Sr0.5Co0.8Fe0.2O3−δ composite membrane, Solid State Ionics, 181 (2010) 1387-1393.

[14] M.B. Choi, S.Y. Jeon, H.J. Hwang, J.Y. Park, S.J. Song, Composite of Ce0.8Gd0.2O2−δ and GdBaCo2O5+δ as oxygen separation membranes, Solid State Ionics, 181 (2010) 1680-1684.

[15] H. Luo, H. Jiang, K. Efimov, F. Liang, H. Wang, J. Caro, CO2-Tolerant Oxygen-Permeable Fe2O3-Ce0.9Gd0.1O2-δ Dual Phase Membranes, Industrial & Engineering Chemistry Research, 50 (2011) 13508-13517.

[16] H. Luo, K. Efimov, H. Jiang, A. Feldhoff, H. Wang, J. Caro, CO2-Stable and Cobalt-Free Dual-Phase Membrane for Oxygen Separation, Angewandte Chemie International Edition, 50 (2011) 759-763.

[17] M. Balaguer, C. Solis, J.M. Serra, Study of the Transport Properties of the Mixed Ionic Electronic Conductor Ce1-xTbxO2-d + Co (x = 0.1, 0.2) and Evaluation As Oxygen-Transport Membrane, Chemistry of Materials, 23 (2011) 2333-2343.

[18] H.A.E. Dole, E.A. Baranova, Ethylene Oxidation in an Oxygen-Deficient Environment: Why Ceria is an Active Support?, Chemcatchem, 8 (2016) 1977-1986.

[19] M.P. Lobera, M. Balaguer, J. Garcia-Fayos, J.M. Serra, Rare Earth-doped Ceria Catalysts for ODHE Reaction in a Catalytic Modified MIEC Membrane Reactor, Chemcatchem, 4 (2012) 2102-2111.

[20] J. Garcia-Fayos, M.P. Lobera, M. Balaguer, J.M. Serra, Catalyst Screening for Oxidative Coupling of Methane Integrated in Membrane Reactors, Frontiers in Materials, 5 (2018).

[21] J.M. Serra, J. Garcia-Fayos, S. Baumann, F. Schulze-Kueppers, W.A. Meulenberg, Oxygen permeation through tape-cast asymmetric all-La0.6Sr0.4Co0.2Fe0.8O3-d membranes, Journal of Membrane Science, 447 (2013) 297-305.

[22] M. Balaguer, J. Garcia-Fayos, C. Solis, J.M. Serra, Fast Oxygen Separation Through SO2- and CO2-Stable Dual-Phase Membrane Based on NiFe2O4-Ce0.8Tb0.2O2-delta, Chemistry of Materials, 25 (2013) 4986-4993.

[23] C. Gaudillere, J. Garcia-Fayos, J. Serra, Enhancing oxygen permeation through hierarchically-structured perovskite membranes elaborated by freeze-casting, Journal of Materials Chemistry A, (2013).

[24] J. Garcia-Fayos, M. Balaguer, J.M. Serra, Dual-Phase Oxygen Transport Membranes for Stable Operation in Environments Containing Carbon Dioxide and Sulfur Dioxide, ChemSusChem, 8 (2015) 4242-4249.

[25] Z. Shao, G. Xiong, H. Dong, W. Yang, L. Lin, Synthesis, oxygen permeation study and membrane performance of a Ba0.5Sr0.5Co0.8Fe0.2O3−δ oxygen-permeable dense ceramic reactor for partial oxidation of methane to syngas, Separation and Purification Technology, 25 (2001) 97-116.

[26] A. Yan, B. Liu, Y. Dong, Z. Tian, D. Wang, M. Cheng, A temperature programmed desorption investigation on the interaction of Ba0.5Sr0.5Co0.8Fe0.2O3−δ perovskite oxides with CO2 in the absence and presence of H2O and O2, Applied Catalysis B: Environmental, 80 (2008) 24-31.

[27] C. Gaudillere, J. Garcia-Fayos, M. Balaguer, J.M. Serra, Enhanced Oxygen Separation through Robust Freeze-Cast Bilayered Dual-Phase Membranes, Chemsuschem, 7 (2014) 2554-2561.

[28] W.H. Weber, K.C. Hass, J.R. McBride, Raman study of CeO_{2}: Second-order scattering, lattice dynamics, and particle-size effects, Physical Review B, 48 (1993) 178-185.

[29] S. Wang, W. Wang, J. Zuo, Y. Qian, Study of the Raman spectrum of CeO2 nanometer thin films, Materials Chemistry and Physics, 68 (2001) 246-248.

[30] M. Guo, J. Lu, Y. Wu, Y. Wang, M. Luo, UV and Visible Raman Studies of Oxygen Vacancies in Rare-Earth-Doped Ceria, Langmuir, 27 (2011) 3872-3877.

[31] L. Meng, A.-P. Jia, J.-Q. Lu, L.-F. Luo, W.-X. Huang, M.-F. Luo, Synergetic Effects of PdO Species on CO Oxidation over PdO-CeO2 Catalysts, Journal of Physical Chemistry C, 115 (2011) 19789-19796.

[32] C. Yacou, J. Sunarso, C.X.C. Lin, S. Smart, S. Liu, J.C. Diniz da Costa, Palladium surface modified La0.6Sr0.4Co0.2Fe0.8O3−δ hollow fibres for oxygen separation, Journal of Membrane Science, 380 (2011) 223-231.